A COARSE MESH TRANSPORT METHOD WITH GENERAL SOURCE TREATMENT FOR MEDICAL PHYSICS

A Thesis
Presented to
The Academic Faculty

By

Robert M. Hayward

In Partial Fulfillment
Of the Requirements for the Degree
Master of Science in Medical Physics

Georgia Institute of Technology
December 2009

A COARSE MESH TRANSPORT METHOD WITH GENERAL SOURCE TREATMENT FOR MEDICAL PHYSICS

Approved by:

Professor Farzad Rahnema, Advisor
Department of Nuclear and Radiological
Engineering and Medical Physics
Georgia Institute of Technology

Dr. Dingkang Zhang
Department of Nuclear and Radiological
Engineering and Medical Physics
Georgia Institute of Technology

Professor Chris Wang
Department of Nuclear and Radiological
Engineering and Medical Physics
Georgia Institute of Technology

Date Approved: October 28, 2009

To my wife,

Erin,

for her love and support.

ACKNOWLEDGEMENTS

I want to thank Dr. Rahnema and Dr. Zhang for valuable discussions, guidance, and insight.

TABLE OF CONTENTS

ACKNOWLEDGEMENTS iv

LIST OF TABLES vii

LIST OF FIGURES viii

SUMMARY ix

I INTRODUCTION 1

1.1 Motivation 1

1.2 Current Methods 1

1.3 A New Method 2

II PREVIOUS WORK 3

2.1 Current Methods 3

2.1.1 Monte Carlo 3

2.1.2 Convolution-Superposition 3

2.1.3 Deterministic 4

2.2 COMET 4

III METHOD 6

3.1 Quantities of Interest 6

3.1.1 Angular Flux 6

3.1.2 Kerma Rate 6

3.2 Collided-Uncollided Transport Equations 7

3.3 Integral Transport 8

3.4 COMET Method 9

IV NUMERICAL IMPLEMENTATION 11

4.1 Calculation of Uncollided Angular Flux, ψ^u 11

4.2 Calculation of Volume-Source Response Functions, Q_i^m 12

4.3 Calculation of Surface-Boundary Response Functions, R_{is}^n 12

4.4 Iteration on Boundary Conditions 14

V RESULTS 17

VI DISCUSSION 28

6.1 Sources of Error 28

6.2 Suggestions for Future Work 29

6.3 Conclusion 30

REFERENCES 31

LIST OF TABLES

1 Parameters Used for COMET solution 18

2 Error Summary 19

3 Running Time Comparison 26

LIST OF FIGURES

1 Beam Energy Spectrum, f(E) 18

2 Specific Kerma Distribution at x=10cm 20

3 Error in Kerma at x=10cm 21

4 Axial Kerma Distributions from the Reference Solution 22

5 Axial Kerma Distributions from the COMET Solution 23

6 Error in Axial Kerma Distributions in Units of K_{max} 24

7 Relative Error in Axial Kerma Distributions 25

8 Percent Depth Kerma (PDK) 26

9 Beam Profiles 27

SUMMARY

The Coarse-Mesh Transport Method (COMET) is a method developed by the Computational Reactor and Medical Physics Group at Georgia Tech. Its original application was neutron transport for nuclear reactor modeling. COMET has since been shown to be effective for coupled photon-electron transport calculations where the goal is to determine the energy deposition of a photon beam. So far COMET can simulate a mono-directional, mono-energetic, spatially-flat photon beam. The goal of this thesis will be to extend COMET by adding a generalized source treatment. The new source will be able to simulate beams that vary in intensity as a function of position, angle, and energy. EGSnrc will be used to verify the accuracy of the new method for 3D photon kerma calculations.

CHAPTER I

INTRODUCTION

1.1 Motivation

Radiation therapy is an important tool in cancer treatment. For a successful treatment, it is important to be able to precisely control the radiation dose. Ideally, 100% of the dose would be deposited inside the tumor volume and 0% outside. Unfortunately this is not possible in general. Realistically a compromise must be made in any radiation therapy plan. The opposing goals then become:

- Maximize dose to tumor volume
- Minimize dose to normal tissue

Modern techniques such as 3-Dimensional Conformal Radiotherapy, Intensity Modulated Radiotherapy, and Helical Tomotherapy are used to take this balance to the edge. In practice, the uncertainty associated with dose calculation is a limiting factor. Boyer and Shultheiss concluded that a reduction in dose uncertainty of 1% would result in an increase in the complication-free tumor control (refered to by the authors as *cure*) rate of 2% [6]. The need for accurate dose calculation is clear.

1.2 Current Methods

There is currently a great divide in dose calculation algorithms. On one end of the spectrum, there is the Monte Carlo (MC) method. The MC method is capable of simulating dose using detailed physical models in complex geometry, but these capabilities come at the cost of speed. At present, the MC method is too computationally intensive to be used in treatment planning. It does, however, serve as a benchmark for new dose calculation algorithms [3].

On the more practical side is the Convolution-Superposition (CS) class of methods. In general, this type of method is based on a photon interaction kernel within an infinite, homogeneous water phantom. Depending on the method, this kernel is either a point kernel or a pencil kernel. The methods differ mainly in their strategies for distributing energy from the primary photon interaction site while correcting for heterogeneity. In general, CS methods are very fast, and this is their main utility [2].

There are also a few researchers who have attempted to solve the Boltzmann Transport Equation (BTE) directly using the discrete ordinates method. Such solutions, while theoretically rigorous, tend to be nearly as computationally intensive as the MC method, and are thus not used in practice [7].

1.3 A New Method

In this text, a novel method to solve the steady-state, linear BTE for photons will be presented. The method is based on a combination of the Method of Characteristics (MOC) and of the heterogeneous coarse-mesh transport method (COMET). The MOC is used to decompose the solution into collided and uncollided components. This decomposition allows the method to handle source terms that are applicable to medical physics. The uncollided component is solved for by analytically inverting the streaming-collision operator. The collided component is solved using the COMET method. The COMET method was originally developed for nuclear reactor computations [9]. It has since been shown to be effective in coupled photon-electron transport using a spatially flat source [20]. By making use of precomputation the new method is able to achieve results comparable to MC in a fraction of the time. In the text that follows, the details of this method are explained fully. Additionally, the method is implemented, and a comparison is made with the EGSnrc MC code.

CHAPTER II

PREVIOUS WORK

2.1 Current Methods

2.1.1 Monte Carlo

The EGSnrc code system is used extensively in this work [11]. User codes are developed to calculate reference solutions, volume-source response functions, and surface-boundary response functions.

2.1.2 Convolution-Superposition

Convolution-Superposition methods get their name from the way they calculate dose. In general, a relationship of the form

$$D(\vec{r}) = \int_V \mathrm{d}\vec{r'}\Phi(\vec{r'})k(\vec{r},\vec{r'}) \tag{1}$$

is used where D is dose, Φ is the primary photon fluence (or some closely related quantity such as terma), and k is the so-called convolution kernel or "dose spread array". $k(\vec{r},\vec{r'})$ gives the dose that results at a point $\vec{r}$ from a unit primary fluence at point $\vec{r'}$.

Mackie et al. calculated this kernel with an MC method by tallying dose in a cartesian grid about a single point of photon interaction in an infinite water phantom. By approximating the kernel as spatially invariant, that is $k(\vec{r},\vec{r'}) = k(\vec{r}-\vec{r'})$, the Fast Fourier Transform can be used to quickly perform this convolution. Corrections are then made for beam divergence and heterogeneity [13].

In the general case, where one does not assume a spatially invariant kernel, the computation becomes much more difficult. In this case, the calculation is a superposition rather than a convolution. For an array of N^3 voxels, $O(N^6)$ work is required to compute the dose. As a faster alternative, Ahnesjö et al. introduced a pencil beam model. In this case, a 2-D

kernel of the form

$$k(r,z) = \frac{A_z e^{-a_z r}}{r} + \frac{B_z e^{-b_z r}}{r} \tag{2}$$

is used where r is the radius from the pencil beam axis, z is the depth, and A_z, a_z, B_z, and b_z are z-dependent parameters found by fit to Monte Carlo calculation. A_z and a_z characterize the relatively long-range secondary photon transport while B_Z and b_z characterize the transport of electrons and low-energy photons. This is a good approximation for photons, but difficult to justify theoretically for electrons.

The Collapsed Cone Convolution (CCC) is similar [1]. Rather than a 2D pencil kernel, CCC uses a 3D point kernel of the form

$$k(r,\Theta) = \frac{A_\Theta e^{-a_\Theta r}}{r^2} + \frac{B_\Theta e^{-b_\Theta r}}{r^2} \tag{3}$$

combined with a discrete ordinates approximation. The main drawback associated with this method is similar to that of the pencil beam superposition. That is the empirical approximation of electron "attenuation" is not rigorously justified. Additionally the solutions obtained with CCC may exhibit ray effects. The rays tend to cancel one another when the terma distribution is smooth. For more on the class of superposition-convolution methods, especially techniques for heterogeneity correction, see the review by Ahnesjö [2].

2.1.3 Deterministic

Some attention has been given to discrete-ordinates based deterministic methods for dose calculation [2, 18, 19]. In general these methods take time on the order of Monte Carlo, but struggle with deterministic approximations to electron transport.

2.2 COMET

The Coarse Mesh Transport method has been previously applied to photon-only transport [15] and to coupled photon-electron transport [5]. Extensive testing has been performed and good agreement with Monte Carlo has been shown. All previous testing, however, has

been for 2D phantom geometry with a spatially-flat, perpendicularly-incident, monoenergetic source. This limits its applicability to clinical treatment planning. The current work extends the COMET method to handle more general source terms for problems with 3D phantom geometry.

CHAPTER III

METHOD

3.1 Quantities of Interest

Before we get into the details of the method, we must define the quantities we will use to describe the radiation field.

3.1.1 Angular Flux

We shall use *angular flux*, ψ, to describe the distribution of photons as follows:

$$\psi(\vec{r}, E, \hat{\Omega})\, dV\, dE\, d\hat{\Omega}\, dt = \text{the expectation value of the total track length of all photons in the volume element } dV \text{ about point } \vec{r} \text{ with energies between } E \text{ and } E + dE \text{ moving in the cone of directions } d\hat{\Omega} \text{ about } \hat{\Omega} \text{ during } dt.$$

The point $\vec{r}$ will be defined in cartesian coordinates (x, y, z), and the direction vector $\hat{\Omega}$ will be defined by the polar and azimuthal angles (θ, ϕ) respectively. The incremental solid angle, $d\hat{\Omega}$, will be defined $d\hat{\Omega} = \sin\theta\, d\theta\, d\phi$; this yields the normalization $\int d\hat{\Omega} = 4\pi$. The units of angular flux are $\psi(\vec{r}, E, \hat{\Omega}) = \left[\text{photons} \cdot \text{cm}^{-2}\text{MeV}^{-1}\text{sr}^{-1}\text{s}^{-1}\right]$. This is equivalent to the *differential flux density* or *differential fluence rate*[4].

3.1.2 Kerma Rate

In radiation therapy, dose is deposited by charged particles. Since this work concerns only photon transport, the dose rate cannot be calculated. Instead the *kerma rate*, K, will be calculated from the angular flux as

$$K(\vec{r}) = \int_0^\infty dE \int_{4\pi} d\hat{\Omega}\, \frac{\mu_{tr}(\vec{r}, E)}{\rho(\vec{r})}\, E \cdot \psi(\vec{r}, E, \hat{\Omega}). \tag{4}$$

μ_{tr}/ρ is the *mass energy-transfer coefficient*, which has units of $[\mathrm{cm}^2\mathrm{g}^{-1}]$. This gives kerma rate units of $\left[\mathrm{MeV}\cdot\mathrm{g}^{-1}\mathrm{s}^{-1}\right]$ [4].

3.2 Collided-Uncollided Transport Equations

Photons obey the steady-state Boltzmann Transport Equation (BTE) which can be written

$$\hat{\Omega}\cdot\vec{\nabla}\psi(\vec{\mathrm{r}},E,\hat{\Omega}) \;+\; \sigma_t(\vec{\mathrm{r}},E)\psi(\vec{\mathrm{r}},E,\hat{\Omega}) = \int_0^\infty dE' \int_{4\pi} \mathrm{d}\hat{\Omega}'\,\sigma_s(\vec{\mathrm{r}},E'\to E,\hat{\Omega}'\cdot\hat{\Omega})\psi(\vec{\mathrm{r}},E',\hat{\Omega}') \;+\; q(\vec{\mathrm{r}},E,\hat{\Omega}) \tag{5}$$

with the boundary condition

$$\psi(\vec{\mathrm{r}},E,\hat{\Omega}) = 0 \qquad \text{for} \qquad \vec{\mathrm{r}}\in\partial V \quad \text{and} \quad \hat{\mathrm{n}}\cdot\hat{\Omega} < 0. \tag{6}$$

$\sigma_t(\vec{\mathrm{r}},E)$ is the *photon interaction cross section* or *attenuation coefficient*. σ_t has units of $\left[\mathrm{cm}^{-1}\right]$. $\sigma_s(\vec{\mathrm{r}},E'\to E,\hat{\Omega}'\cdot\hat{\Omega})$ is the *photon scattering cross section*; it describes the probability per distance that a photon moving with energy and direction $(E',\hat{\Omega}')$ undergoes a scattering interaction and emerges with energy and direction $(E,\hat{\Omega})$. σ_s has units of $\left[\mathrm{cm}^{-1}\mathrm{MeV}^{-1}\mathrm{sr}^{-1}\right]$. $q(\vec{\mathrm{r}},E,\hat{\Omega})$ is an inhomogeneous source term with units $\left[\mathrm{photons}\cdot\mathrm{cm}^{-3}\mathrm{MeV}^{-1}\mathrm{sr}^{-1}\mathrm{s}^{-1}\right]$ [12]. For the purpose of this paper, q will represent the fluence of photons from the linear accelerator (linac) head. This problem is defined in the region V with boundary ∂V. $\hat{\mathrm{n}}$ is defined as an outward normal unit vector on ∂V. For the sake of brevity, it is convenient to rewrite equation (5) in operator notation as

$$(\mathbf{L}+\mathbf{C})\psi(\vec{\mathrm{r}},E,\hat{\Omega}) = \mathbf{S}\psi(\vec{\mathrm{r}},E,\hat{\Omega}) + q(\vec{\mathrm{r}},E,\hat{\Omega}) \tag{7}$$

where

$$\begin{aligned}
\mathbf{L}\psi(\vec{\mathrm{r}},E,\hat{\Omega}) &= \hat{\Omega}\cdot\nabla\psi(\vec{\mathrm{r}},E,\hat{\Omega}),\\
\mathbf{C}\psi(\vec{\mathrm{r}},E,\hat{\Omega}) &= \sigma_t(\vec{\mathrm{r}},E)\psi(\vec{\mathrm{r}},E,\hat{\Omega}),\ \text{and}\\
\mathbf{S}\psi(\vec{\mathrm{r}},E,\hat{\Omega}) &= \int_0^\infty dE' \int_{4\pi} \mathrm{d}\hat{\Omega}'\,\sigma_s(\vec{\mathrm{r}},E'\to E,\hat{\Omega}'\cdot\hat{\Omega})\psi(\vec{\mathrm{r}},E',\hat{\Omega}')
\end{aligned}$$

are the *leakage*, *collision*, and *scattering* operators respectively. We can write ψ as the sum

$$\psi(\vec{\mathrm{r}}, E, \hat{\Omega}) = \psi^u(\vec{\mathrm{r}}, E, \hat{\Omega}) + \psi^c(\vec{\mathrm{r}}, E, \hat{\Omega})$$

where ψ^u is the *uncollided angular flux*, which represents photons that have not undergone any collisions since being emitted from the source, and ψ^c is the *collided angular flux*, which represents photons that have undergone at least one collision. With this substitution, equation (7) separates into the pair of equations

$$(\mathbf{L} + \mathbf{C})\psi^u(\vec{\mathrm{r}}, E, \hat{\Omega}) = q(\vec{\mathrm{r}}, E, \hat{\Omega}) \tag{8}$$

$$(\mathbf{L} + \mathbf{C})\psi^c(\vec{\mathrm{r}}, E, \hat{\Omega}) = \mathbf{S}\psi^c(\vec{\mathrm{r}}, E, \hat{\Omega}) + q_c(\vec{\mathrm{r}}, E, \hat{\Omega}) \tag{9}$$

where $q_c(\vec{\mathrm{r}}, E, \hat{\Omega}) \equiv \mathbf{S}\psi^u(\vec{\mathrm{r}}, E, \hat{\Omega})$ is the once-collided source term. At first glance it appears that this decomposition does little to help solve for the angular flux, ψ, since solving equation (9) for ψ^c appears to be just as difficult as solving equation (7) for ψ; that is without even considering the need to solve equation (8). The key difference between solving the BTE (equation (7)) and the system of equations (8 and 9) is related to the difference between the respective source terms q and q_c.

3.3 Integral Transport

Solving equation (8) for ψ^u results in the relationship $\psi^u(\vec{\mathrm{r}}, E, \hat{\Omega}) = (\mathbf{L}+\mathbf{C})^{-1}q(\vec{\mathrm{r}}, E, \hat{\Omega})$. The operator $\mathbf{T} \equiv (\mathbf{L} + \mathbf{C})^{-1}$ is the integral transport operator, which can be defined by

$$\mathbf{T}q(\vec{\mathrm{r}}, E, \hat{\Omega}) \equiv \int_V \frac{e^{-\tau(\vec{\mathrm{r}},\vec{\mathrm{r}'},E)}}{\left|\vec{\mathrm{r}} - \vec{\mathrm{r}'}\right|^2} \delta\left(\hat{\Omega} \cdot \frac{\vec{\mathrm{r}} - \vec{\mathrm{r}'}}{\left|\vec{\mathrm{r}} - \vec{\mathrm{r}'}\right|}\right) q(\vec{\mathrm{r}'}, E, \hat{\Omega})\, \mathrm{d}V' \tag{10}$$

where $\mathrm{d}V'$ is the volume element about $\vec{\mathrm{r}'}$, and the directional Dirac delta function is defined as $\delta(\hat{\Omega} \cdot \hat{\Omega}') \equiv \delta(\theta - \theta')\delta(\phi - \phi')$. τ is the *optical depth*

$$\tau(\vec{r}, \vec{r} - R\hat{\Omega}, E) = \int_0^R \mathrm{d}R'\, \sigma_t(\vec{r} - R'\hat{\Omega}, E) \quad \text{for} \quad R > 0 \tag{11}$$

[18, 12]. Since it is straightforward to calculate ψ^u, the challenge becomes solving equation (9) for ψ^c.

3.4 COMET Method

Recall equation (9)

$$(\mathbf{L} + \mathbf{C})\psi^c(\vec{\mathrm{r}}, E, \hat{\Omega}) = \mathbf{S}\psi^c(\vec{\mathrm{r}}, E, \hat{\Omega}) + q_c(\vec{\mathrm{r}}, E, \hat{\Omega})$$

defined on V. This equation shall be referred to as the global problem. The first step in application of the COMET method is division of the domain, V into a set of I coarse meshes, $\{V_i\}$, such that

$$V = \bigcup_{i=1}^{I} V_i. \tag{12}$$

On each coarse mesh, a local transport problem is defined by

$$(\mathbf{L} + \mathbf{C})\varphi_i(\vec{\mathrm{r}}, E, \hat{\Omega}) = \mathbf{S}\varphi_i(\vec{\mathrm{r}}, E, \hat{\Omega}) + q_i(\vec{\mathrm{r}}, E, \hat{\Omega}). \tag{13}$$

If the local problem source term and boundary conditions satisfy

$$q_i(\vec{\mathrm{r}}, E, \hat{\Omega}) = q_c(\vec{\mathrm{r}}, E, \hat{\Omega}) \qquad \text{for} \quad \vec{\mathrm{r}} \in V_i \tag{14}$$

$$\varphi_i(\vec{\mathrm{r}}, E, \hat{\Omega}) = \psi^c(\vec{\mathrm{r}}, E, \hat{\Omega}) \qquad \text{for} \quad \vec{\mathrm{r}} \in \partial V_i \quad \text{and} \quad \hat{\mathrm{n}}_\mathrm{i} \cdot \hat{\Omega} < 0 \tag{15}$$

then the set of local solutions, $\{\varphi_i\}$, form an exact solution to the global problem [9, 14].

Let Λ_i denote the full phase space within the mesh V_i. Let ω_i^- denote the portion of phase space such that $\vec{\mathrm{r}} \in \partial V_i$ and $\hat{\mathrm{n}}_\mathrm{i} \cdot \hat{\Omega} < 0$, and let ω_i^+ denote the portion of phase space such that $\vec{\mathrm{r}} \in \partial V_i$ and $\hat{\mathrm{n}}_\mathrm{i} \cdot \hat{\Omega} > 0$. Further, let $\omega_{is}^\pm$ denote the restriction of $\omega_i^\pm$ to surface s.

Let the *volume-source response function*, Q_i^m, be defined as the solution to the local problem

$$(\mathbf{L} + \mathbf{C})Q_i^m(\vec{\mathrm{r}}, E, \hat{\Omega}) = \mathbf{S}Q_i^m(\vec{\mathrm{r}}, E, \hat{\Omega}) + \eta^m(\vec{\mathrm{r}}, E, \hat{\Omega}) \tag{16}$$

with the boundary condition

$$Q_i^m(\vec{\mathrm{r}}, E, \hat{\Omega}) = 0 \quad \text{for} \quad (\vec{\mathrm{r}}, E, \hat{\Omega}) \in \omega_i^- \tag{17}$$

where η^m represents the m^{th} function of a complete set of orthonormal functions defined on Λ_i. An arbitrary collided source term, q_c, can thus be approximated by

$$q_c(\vec{\mathrm{r}}, E, \hat{\Omega}) \approx \sum_{m=0}^{M} a_i^m \eta^m(\vec{\mathrm{r}}, E, \hat{\Omega}) \tag{18}$$

where

$$a_i^m = \int_{\Lambda_i} \eta^m(\vec{\mathrm{r}}, E, \hat{\Omega}) q_c(\vec{\mathrm{r}}, E, \hat{\Omega}). \tag{19}$$

Similarly, let the *surface-boundary response function*, R_{is}^n, be defined as the solution to the local problem

$$(\mathbf{L} + \mathbf{C}) R_{is}^n(\vec{\mathrm{r}}, E, \hat{\Omega}) = \mathbf{S} R_{is}^n(\vec{\mathrm{r}}, E, \hat{\Omega}) \tag{20}$$

with the boundary condition

$$R_{is}^n(\vec{\mathrm{r}}, E, \hat{\Omega}) = \begin{cases} \Gamma^n(\vec{\mathrm{r}}, E, \hat{\Omega}), & (\vec{\mathrm{r}}, E, \hat{\Omega}) \in \omega_{is}^- \\ 0, & (\vec{\mathrm{r}}, E, \hat{\Omega}) \in \left(\omega_i^- - \omega_{is}^-\right) \end{cases} \tag{21}$$

where Γ^n represents the n^{th} function of a complete set of orthonormal functions defined on ω_{is}^-. This means that arbitrary incoming boundary conditions, $\psi^c(\vec{\mathrm{r}}, E, \hat{\Omega}) = f(\vec{\mathrm{r}}, E, \hat{\Omega})$ for $(\vec{\mathrm{r}}, E, \hat{\Omega}) \in \omega_{is}^-$, can be approximated by

$$f(\vec{\mathrm{r}}, E, \hat{\Omega}) \approx \sum_{n=0}^{N} b_{is}^n \Gamma^n(\vec{\mathrm{r}}, E, \hat{\Omega}) \tag{22}$$

with

$$b_{is}^n = \int_{\omega_{is}^-} \Gamma^n(\vec{\mathrm{r}}, E, \hat{\Omega}) f(\vec{\mathrm{r}}, E, \hat{\Omega}) \tag{23}$$

By superimposing linear combinations of Q_i^m and R_{is}^n, the solution of any fixed source problem can be created. The local solutions are coupled by requiring that the angular flux be continuous across mesh boundaries, and the global problem can be solved by iteratively enforcing this coupling. The only approximations made in this approach are that the series $\{a_i^m\}$ and $\{b_i^n\}$ are truncated at finite values of m and n respectively.

CHAPTER IV

NUMERICAL IMPLEMENTATION

In this work, all kerma calculations are performed on a regular array of cube-shaped voxels. This is common in radiation therapy because the patient geometry is defined by a voxelized CT dataset. The coarse meshes are defined to coincide with these voxels for simplicity.

4.1 Calculation of Uncollided Angular Flux, ψ^u

For the sake of simplicity, assume that the linac photon beam is well-approximated by a point source. That is

$$q(\vec{\mathrm{r}}, E, \hat{\Omega}) = \delta(\vec{\mathrm{r}} - \vec{\mathrm{r}_\mathrm{s}}) q(\vec{\mathrm{r}_\mathrm{s}}, E, \hat{\Omega}). \tag{24}$$

This may seem to be a severe restriction, but note that any arbitrary source term may be constructed by superposition of point sources. Using equation (10), ψ^u can be written

$$\begin{aligned} \psi^u(\vec{\mathrm{r}}, E, \hat{\Omega}) &= \mathbf{T} q(\vec{\mathrm{r}}, E, \hat{\Omega}) \\ &= \frac{e^{-\tau(\vec{\mathrm{r}}, \vec{\mathrm{r}_\mathrm{s}}, E)}}{\left|\vec{\mathrm{r}} - \vec{\mathrm{r}_\mathrm{s}}\right|^2} \delta\left(\hat{\Omega} \cdot \frac{\vec{\mathrm{r}} - \vec{\mathrm{r}_\mathrm{s}}}{\left|\vec{\mathrm{r}} - \vec{\mathrm{r}_\mathrm{s}}\right|}\right) q(\vec{\mathrm{r}_\mathrm{s}}, E, \hat{\Omega}). \end{aligned} \tag{25}$$

By discretizing the energy variable into bins, equation (25) becomes

$$\psi^u_g(\vec{\mathrm{r}}, \hat{\Omega}) = \frac{e^{-\tau_g(\vec{\mathrm{r}}, \vec{\mathrm{r}_\mathrm{s}})}}{\left|\vec{\mathrm{r}} - \vec{\mathrm{r}_\mathrm{s}}\right|^2} \delta\left(\hat{\Omega} \cdot \frac{\vec{\mathrm{r}} - \vec{\mathrm{r}_\mathrm{s}}}{\left|\vec{\mathrm{r}} - \vec{\mathrm{r}_\mathrm{s}}\right|}\right) q_g(\vec{\mathrm{r}_\mathrm{s}}, \hat{\Omega}) \tag{26}$$

where

$$\tau_g(\vec{\mathrm{r}}, \vec{\mathrm{r}_\mathrm{s}}) = \tau(\vec{\mathrm{r}}, \vec{\mathrm{r}_\mathrm{s}}, E_g) \tag{27}$$

$$q_g(\vec{\mathrm{r}_\mathrm{s}}, \hat{\Omega}) = \frac{1}{E_g} \int_{E_{g-1/2}}^{E_{g+1/2}} \mathrm{d}E' E' q(\vec{\mathrm{r}_\mathrm{s}}, E', \hat{\Omega}). \tag{28}$$

τ_g can be evaluated using the Siddon Algorithm or similar [17, 10, 21].

Finally, define

$$w_{i,g} = \int_{4\pi} \mathrm{d}\hat{\Omega} \int_{V_i} \mathrm{d}V \, \sigma_t(E_g) \psi^u_g(\vec{\mathrm{r}}, \hat{\Omega}). \tag{29}$$

4.2 Calculation of Volume-Source Response Functions, Q_i^m

Recall equation (16)

$$(\mathbf{L}+\mathbf{C})Q_i^m(\vec{\mathrm{r}},E,\hat{\Omega}) = \mathbf{S}Q_i^m(\vec{\mathrm{r}},E,\hat{\Omega}) + \eta^m(\vec{\mathrm{r}},E,\hat{\Omega}).$$

Choose

$$\eta^m(\vec{\mathrm{r}},E,\hat{\Omega}) \equiv \mathbf{S}\left[\delta(E-E_m)\delta(\hat{\Omega}\cdot\hat{\mathrm{z}})\right]. \tag{30}$$

The physical interpretation of this source is that photons with energy E_m, moving in the positive z-direction, are forced to make their first collisions uniformly throughout the volume of the voxel. Since this approximation forces all photons to move parallel to the beam's central axis, it works best for small field sizes and large source-to-surface distances (SSDs).

The solutions, Q_i^m, are calculated with an EGSnrc user code. Tallies were scored for

$$k[Q_i^m] = \int_{V_i}\mathrm{d}V\int_0^\infty \mathrm{d}E\int_{4\pi}\mathrm{d}\hat{\Omega}\,\frac{\mu_{tr}(\vec{\mathrm{r}},E)}{\rho(\vec{\mathrm{r}})}\,E\cdot Q_i^m(\vec{\mathrm{r}},E,\hat{\Omega}) \tag{31}$$

and

$$j_s^n[Q_i^m] = \int_{\omega_{is}^+}\Gamma^n(\vec{\mathrm{r}},E,\hat{\Omega})Q_i^m(\vec{\mathrm{r}},E,\hat{\Omega}). \tag{32}$$

Let M_η denote the number of terms in the source expansion. In other words $m \in \left\{0,1,\ldots,M_\eta-1\right\}$.

4.3 Calculation of Surface-Boundary Response Functions, R_{is}^n

Recall equation (20) and equation (21)

$$(\mathbf{L}+\mathbf{C})R_{is}^n(\vec{\mathrm{r}},E,\hat{\Omega}) = \mathbf{S}R_{is}^n(\vec{\mathrm{r}},E,\hat{\Omega})$$

$$R_{is}^n(\vec{\mathrm{r}},E,\hat{\Omega}) = \begin{cases} \Gamma^n(\vec{\mathrm{r}},E,\hat{\Omega}), & (\vec{\mathrm{r}},E,\hat{\Omega}) \in \omega_{is}^- \\ 0, & (\vec{\mathrm{r}},E,\hat{\Omega}) \in \left(\omega_i^- - \omega_{is}^-\right). \end{cases}$$

Choose Γ^n to be a product of 5 orthornormal basis functions scaled by the factor $\frac{1}{\cos\theta}$

$$\Gamma^n(\vec{\mathrm{r}},E,\hat{\Omega}) \equiv \left(\frac{1}{\cos\theta}\right)(\mathrm{side}_{\ell_s}(\vec{\mathrm{r}}))\,U_{\ell_u}^{[u_{min},u_{max}]}(u)\cdot \tag{33}$$

$$U_{\ell_v}^{[v_{min},v_{max}]}(v)U_{\ell_E}^{[E_{min},E_{max}]}(E)U_{\ell_\theta}^{[0,1]}(\cos\theta)V_{\ell_\phi}^{[-\pi,\pi]}(\phi).$$

In the above equation, n is a composite index that results from flattening the 6 indices ℓ_s, ℓ_u, ℓ_v, ℓ_E, ℓ_θ, and ℓ_ϕ into a single index. Each term in the expansion can be factored into 5 independent terms, each a function of one variable, each corresponding to a single dimension of the phase space. The 2-vector (u, v) describes the local coordinates on surface ℓ_s, and function, side_{ℓ_s}, restricts the expansion to surface ℓ_s; that is:

$$\text{side}_{\ell_s}(\vec{\mathrm{r}}) \equiv \begin{cases} 1 & ,\vec{\mathrm{r}} \text{ is a coordinate on surface } \ell_s \\ 0 & ,\text{otherwise.} \end{cases}$$

$U_{\ell_\xi}^{[\xi_{min},\xi_{max}]}(\xi)$ is a shifted and normalized Legendre polynomial defined by

$$U_{\ell_\xi}^{[\xi_{min},\xi_{max}]}(\xi) \equiv \sqrt{\frac{2\ell_\xi + 1}{\xi_{max} - \xi_{min}}} P_{\ell_\xi}\left(2\frac{\xi - \xi_{min}}{\xi_{max} - \xi_{min}} - 1\right)$$

where P_n is a Legendre polynomial with the standard normalization $P_n(1) = 1$. The new polynomial $U_{\ell_\xi}^{[\xi_{min},\xi_{max}]}$ is orthonormal on the interval $[\xi_{min}, \xi_{max}]$ as is easily shown:

$$\begin{aligned}
&\int_{\xi_{min}}^{\xi_{max}} \mathrm{d}\xi V_m^{[\xi_{min},\xi_{max}]}(\xi) V_n^{[\xi_{min},\xi_{max}]}(\xi) \\
&= \frac{\sqrt{(2m+1)(2n+1)}}{\xi_{max} - \xi_{min}} \int_{\xi_{min}}^{\xi_{max}} \mathrm{d}\xi P_m\left(2\frac{\xi - \xi_{min}}{\xi_{max} - \xi_{min}} - 1\right) P_n\left(2\frac{\xi - \xi_{min}}{\xi_{max} - \xi_{min}} - 1\right) \\
&= \frac{\sqrt{(2m+1)(2n+1)}}{2} \int_{-1}^{1} \mathrm{d}x P_m(x) P_n(x) \\
&= \frac{\sqrt{(2m+1)(2n+1)}}{2} \left[\frac{2}{2n+1}\delta_{nm}\right] \\
&= \delta_{nm}
\end{aligned}$$

where δ_{nm} is the Kroenecker delta. $V_{\ell_\xi}^{[\xi_{min},\xi_{max}]}(\xi)$ is a shifted and normalized trigonometric polynomial defined by

$$V_{\ell_\xi}^{[\xi_{min},\xi_{max}]}(\xi) \equiv \frac{1}{\sqrt{\xi_{max} - \xi_{min}}} \begin{cases} 1 & ,\ell_\xi = 0 \\ \sqrt{2}\sin\left((\ell_\xi + 1)\pi\frac{\xi - \xi_{min}}{\xi_{max} - \xi_{min}}\right) & ,\ell_\xi \text{ is odd} \\ \sqrt{2}\cos\left(\ell_\xi\pi\frac{\xi - \xi_{min}}{\xi_{max} - \xi_{min}}\right) & ,\ell_\xi \text{ is even and } \ell_\xi \neq 0. \end{cases}$$

The trigonometric polynomial $V_{\ell_\xi}^{[\xi_{min},\xi_{max}]}$ is orthonormal on the interval $[\xi_{min}, \xi_{max}]$:

$$\int_{\xi_{min}}^{\xi_{max}} \mathrm{d}\xi V_m^{[\xi_{min},\xi_{max}]}(\xi) V_n^{[\xi_{min},\xi_{max}]}(\xi) = \delta_{nm}.$$

Note that the trigonometric expansion is chosen for treating the azimuthal angle. If a Legendre expansion had been used, there would be an artificial discontinuity in the expansion. Since angular flux as a function of ϕ is periodic, a basis that preserves this periodicity is important. The factor of $\frac{1}{\cos\theta}$ in equation (33) makes Γ^n an expansion of the partial current passing through surface ℓ_s. If this were left out, the expansion would be an expansion of angular flux instead.

The solutions, R^n_{is}, are calculated with an EGSnrc user code. Tallies were scored for

$$k[R^n_{is}] = \int_{V_i} \mathrm{d}V \int_0^\infty \mathrm{d}E \int_{4\pi} \mathrm{d}\hat{\Omega}\, \frac{\mu_{tr}(\vec{\mathrm{r}}, E)}{\rho(\vec{\mathrm{r}})}\, E \cdot R^n_{is}(\vec{\mathrm{r}}, E, \hat{\Omega}) \tag{34}$$

and

$$j^{n'}_{s'}[R^n_{is}] = \int_{\omega^+_{is'}} \Gamma^{n'}(\vec{\mathrm{r}}, E, \hat{\Omega}) R^n_{is}(\vec{\mathrm{r}}, E, \hat{\Omega}). \tag{35}$$

Let N_Γ denote the number of terms in the surface expansion. In other words $n \in \{0, 1, \ldots, N_\Gamma - 1\}$.

4.4 Iteration on Boundary Conditions

Define $\vec{\mathrm{J}_0}$ to be the $(6N_\Gamma N_{voxels})$x1 vector

$$\vec{\mathrm{J}_0} = \sum_{m=0}^{M_\eta - 1} \begin{bmatrix} w_{0,m}\, j^0_0[Q^m_0] \\ w_{0,m}\, j^1_0[Q^m_0] \\ \cdots \\ w_{0,m}\, j^{N_\Gamma-1}_0[Q^m_0] \\ w_{0,m}\, j^0_1[Q^m_0] \\ w_{0,m}\, j^1_1[Q^m_0] \\ \cdots \\ w_{0,m}\, j^{N_\Gamma-1}_5[Q^m_0] \\ w_{1,m}\, j^0_0[Q^m_1] \\ \cdots \\ w_{N_{voxels}-1,m}\, j^{N_\Gamma-1}_5[Q^m_{N_{voxels}-1}] \end{bmatrix}. \tag{36}$$

This vector describes the partial current exiting each voxel, i, that results directly from primary photon interactions within that voxel. Let $\mathbf{R^j}_{(i,s)\leftarrow(i',s')}$ be the N_ΓxN_Γ matrix

$$\mathbf{R^j}_{(i,s)\leftarrow(i',s')} = \begin{cases} \begin{pmatrix} j^0_{(s+3)\text{mod}6}[R^0_{i's'}] & \cdots & j^0_{(s+3)\text{mod}6}[R^{N_\Gamma-1}_{i's'}] \\ \vdots & \ddots & \\ j^{N_\Gamma-1}_{(s+3)\text{mod}6}[R^0_{i's'}] & & j^{N_\Gamma-1}_{(s+3)\text{mod}6}[R^{N_\Gamma-1}_{i's'}] \end{pmatrix}, & (i',s') \rightarrow i \\ \mathbf{0}, & \text{otherwise.} \end{cases} \tag{37}$$

The condition $[(i', s') \rightarrow i]$ is met if and only if the current out of surface s' of voxel i' enters voxel i. Let $\mathbf{R^j}$ be the matrix with $(6N_{voxels}\text{x}6N_{voxels})$ blocks defined by

$$\mathbf{R^j} = \begin{pmatrix} \mathbf{R^j}_{(0,0)\leftarrow(0,0)} & \mathbf{R^j}_{(0,0)\leftarrow(0,1)} & \cdots & \mathbf{R^j}_{(0,0)\leftarrow(N_{voxels}-1,5)} \\ \mathbf{R^j}_{(0,1)\leftarrow(0,0)} & \mathbf{R^j}_{(0,1)\leftarrow(0,1)} & & \\ \vdots & & \ddots & \\ \mathbf{R^j}_{(N_{voxels}-1,5)\leftarrow(0,0)} & & & \mathbf{R^j}_{(N_{voxels}-1,5)\leftarrow(N_{voxels}-1,5)} \end{pmatrix}. \tag{38}$$

Note that most entries of $\mathbf{R^j}$ are zero as a consequence of the condition in equation (37).

Let $\vec{\mathrm{J}}^*$ be the current vector that describes the exact solution of the global problem. With this definition in place, one can see that

$$\vec{\mathrm{J}}^* = \mathbf{R^j}\vec{\mathrm{J}}^* + \vec{\mathrm{J}}_0 \tag{39}$$

or equivalently

$$\left(\mathbf{I} - \mathbf{R^j}\right)\vec{\mathrm{J}}^* = \vec{\mathrm{J}}_0. \tag{40}$$

This linear system can be solved with a variety of methods. For the results in this work, a Jacobi iteration is used

$$\vec{\mathrm{J}}_{\mathrm{i+1}} = \mathbf{R^j}\vec{\mathrm{J}}_{\mathrm{i}} + \vec{\mathrm{J}}_0. \tag{41}$$

Define $\vec{\mathrm{K}}_0$ to be the N_{voxels}x1 vector

$$\vec{\mathrm{K}}_0 = \sum_{m=0}^{M_\eta-1} \begin{pmatrix} w_{0,m}\, k[Q^m_0] \\ w_{1,m}\, k[Q^m_1] \\ \cdots \\ w_{N_{voxels}-1,m}\, k[Q^m_{N_{voxels}-1}] \end{pmatrix}. \tag{42}$$

This vector describes the kerma in each voxel, i, that results directly from the interaction of primary photons within voxel i and also from any collisions of resultant photons that have not yet left voxel i.

Let $\mathbf{R^k}_{i\leftarrow(i',s')}$ be the 1xN_Γ matrix

$$\mathbf{R^k}_{i\leftarrow(i',s')} = \begin{cases} \begin{pmatrix} k[R^0_{i's'}] & \dots & k[R^{N-1}_{i's'}] \end{pmatrix}, & (i',s') \rightarrow i \\ \mathbf{0}, & \text{otherwise.} \end{cases} \tag{43}$$

Let $\mathbf{R^k}$ be the matrix with (N_{voxels}x6N_{voxels}) blocks defined by

$$\mathbf{R^k} = \begin{pmatrix} \mathbf{R^k}_{0\leftarrow(0,0)} & \mathbf{R^k}_{0\leftarrow(0,1)} & \dots & \mathbf{R^k}_{0\leftarrow(N_{voxels}-1,5)} \\ \mathbf{R^k}_{1\leftarrow(0,0)} & \mathbf{R^k}_{1\leftarrow(0,1)} & & \\ \vdots & & \ddots & \\ \mathbf{R^k}_{N_{voxels}-1\leftarrow(0,0)} & & & \mathbf{R^k}_{N_{voxels}-1\leftarrow(N_{voxels}-1,5)} \end{pmatrix}. \tag{44}$$

For any given iterate, $\vec{\mathrm{J}}_\mathrm{i}$, one can calculate a corresponding kerma vector

$$\vec{\mathrm{K}}_\mathrm{i} = \mathbf{R^k}\vec{\mathrm{J}}_\mathrm{i} + \vec{\mathrm{K}}_0. \tag{45}$$

The iteration is terminated when $\left\|\vec{\mathrm{K}}_\mathrm{i} - \vec{\mathrm{K}}_{\mathrm{i}-1}\right\|_2 \leq \epsilon \left\|\vec{\mathrm{K}}_0\right\|_2$.

CHAPTER V

RESULTS

A simple benchmark problem is used for the first test case. A 20x20x20cm water phantom with 1x1x1cm voxels is irradiated with photons from a polyenergetic point source. The phantom is placed at source-to-surface distance (SSD) of 80cm. The field size at the phantom surface is 10x10cm. The beam's energy spectrum is given by the piecewise linear PDF

$$f(E) = \begin{cases} \frac{2(E-E_{min})}{(E_{max}-E_{min})(E_{peak}-E_{min})} & , \; E_{min} \leq E \leq E_{peak} \\ \frac{2(E_{max}-E)}{(E_{max}-E_{min})(E_{max}-E_{peak})} & , \; E_{peak} < E \leq E_{max} \\ 0 & , \text{ otherwise} \end{cases}$$

with $E_{min} = 0.01$ MeV, $E_{peak} = 0.5$ MeV, and $E_{max} = 8$ MeV depicted in Figure 1 on the following page. This spectrum is fictional, but it captures much of the character of a generic 8MV linac spectrum [16]. The source term for the beam is

$$q(\vec{r}, E, \hat{\Omega}) = \begin{cases} \frac{4\pi \; f(E) \; \delta(\vec{r}-[0,0,-80])}{\cos\theta \int_{-5}^{5}\int_{-5}^{5} \frac{dx'dy'}{x'^2+y'^2+80^2}} & , \quad |\tan\theta\cos\phi| \leq \frac{5}{80} \quad \text{and} \\ & \quad |\tan\theta\sin\phi| \leq \frac{5}{80} \\ 0 & , \text{otherwise} \end{cases} \tag{46}$$

where θ is the angle with respect to the beam's central axis. The beam's space-angle dependence is constructed so that the current entering the phantom is a spatially-flat, unit current.

The reference solution was calculated with EGSnrc. All kerma values in the reference solution have statistical uncertainty of $1\sigma < 0.5\%$. Because the errors in the COMET solution are significantly higher than this value, propagation of statistical uncertainty through the error analysis is not shown. The COMET solution was calculated with the parameters listed in Table 1 on the next page.

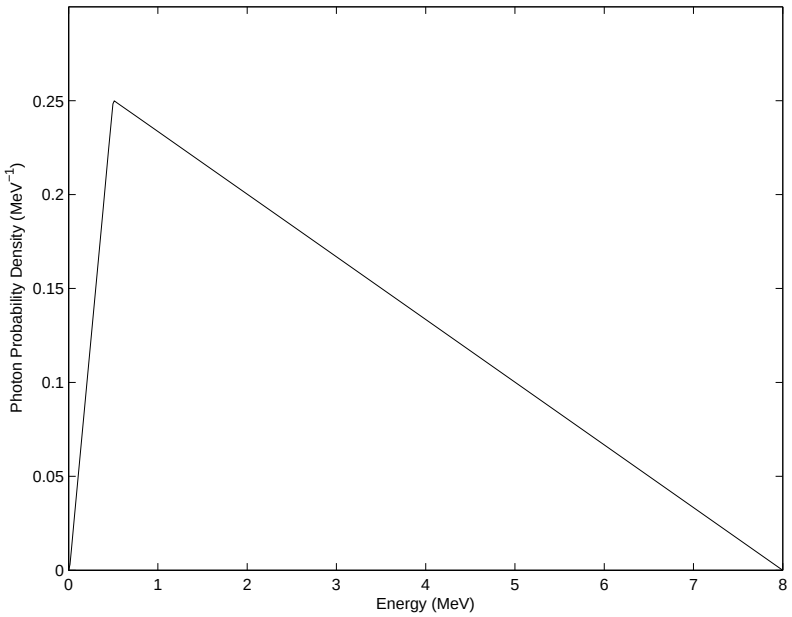

Figure 1: Beam Energy Spectrum, f(E)

Table 1: Parameters Used for COMET solution

parameter	abbreviation	value
number of u-coordinate expansion terms	N_u	3
number of v-coordinate expansion terms	N_v	3
number of energy expansion terms	N_E	3
number of polar expansion terms	N_θ	3
number of azimuthal expansion terms	N_ϕ	3
number of energy bins	G	32
lower energy bound	E_{min}	0.01 MeV
upper energy bound	E_{min}	8.0 MeV
convergence parameter	ϵ	10^{-3}

Table 2: Summary of COMET Solution's Accuracy. $error \equiv K_{COMET} - K_{ref}$.

quantity	**value**	**comment**
$\max \lvert error \rvert$	2.05x10^{-5}	occurs at depth=9.5cm within the beam.
$\frac{\max \lvert error \rvert}{\max(K_{ref})}$	3.30%	
$\frac{\text{rms}(error)}{\max(K_{ref})}$	1.45%	
$\frac{\text{avg}\lvert error \rvert}{\max(K_{ref})}$	1.16%	
$\max \left\lvert \frac{error}{K_{ref}} \right\rvert$	208%	occurs inside a voxel near the phantom's edge at depth=7.5cm.
$\text{rms} \left\lvert \frac{error}{K_{ref}} \right\rvert$	69.3%	
$\text{average} \left\lvert \frac{error}{K_{ref}} \right\rvert$	46.3%	

Figures 2 to 9 on pages 20–27 depict the reference solution, the COMET solution, and the differences between them. Table 2 contains a summary of the COMET solution's accuracy. In terms of relative error, the new method did well inside the boundaries of the beam and did poorly outside these boundaries. This can be seen in Figure 3(b) on page 21. The maximum relative error of 208% occurs on the edge of the phantom at a depth of 7.5cm in a voxel that received just 0.37% of K_{max}. A more relevant picture of the error is provided by looking at the absolute error in units of K_{max} because this scale is typically used in clinical decision making. In this scale, all errors are $\leq 3.3\%$ of K_{max}. This can be seen in Figure 3(a) on page 21. The maximum absolute error occurs in a voxel within the beam at a depth of 9.5cm.

Run times for various calculations are given in Table 3 on page 26. Note that the COMET solution runtime was dominated by the Jacobi iteration; the calculation of the uncollided flux, the initial current vector $\vec{J}_0$, and the initial dose vector $\vec{D}_0$ typically took less than 1 minute combined.

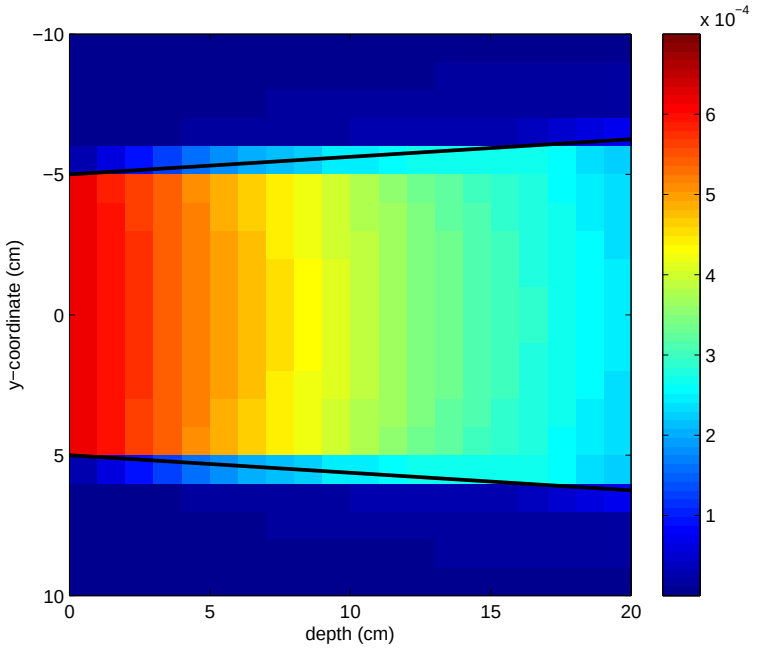

(a) Reference solution

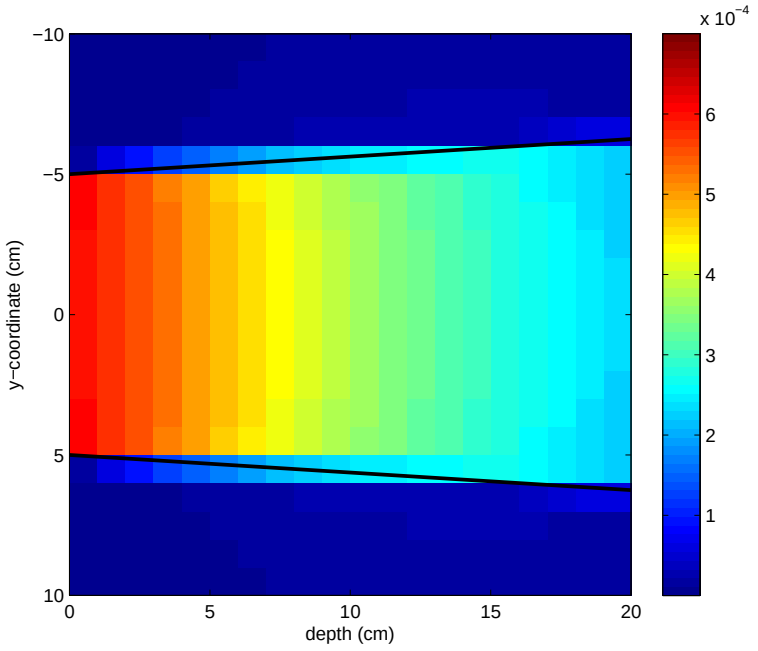

(b) COMET solution

Figure 2: Specific kerma [MeV g^{-1} $photon^{-1}$] on the plane defined by $x = 10$cm. The black line denotes the beam edge.

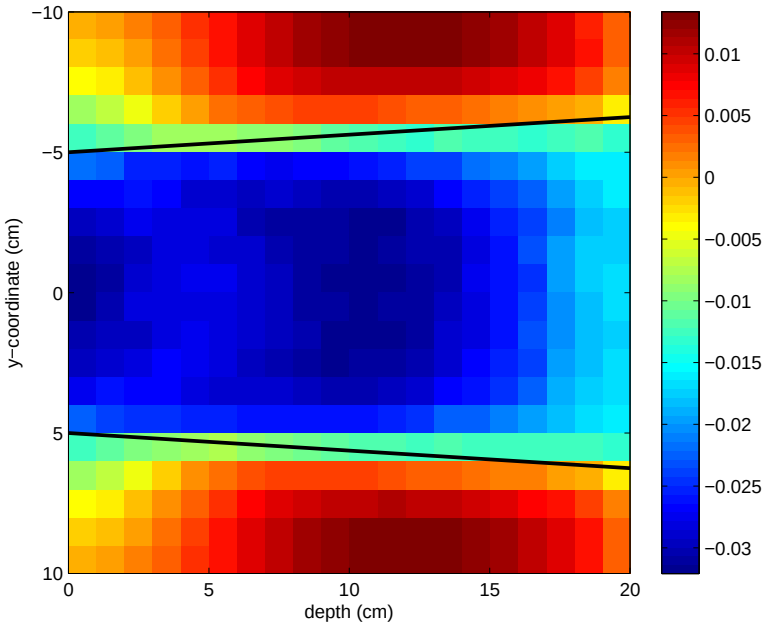

(a) Error (units of K_{max})

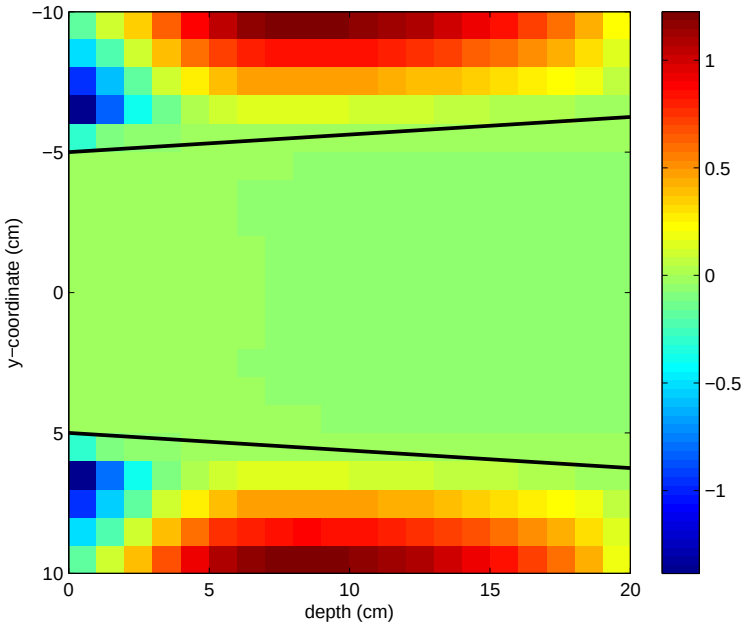

(b) Relative error

Figure 3: Error in kerma on the plane defined by $x = 10$cm. The black line denotes the beam edge.

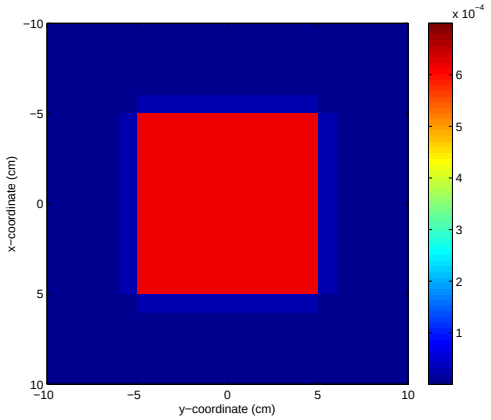

(a) depth=0.5cm

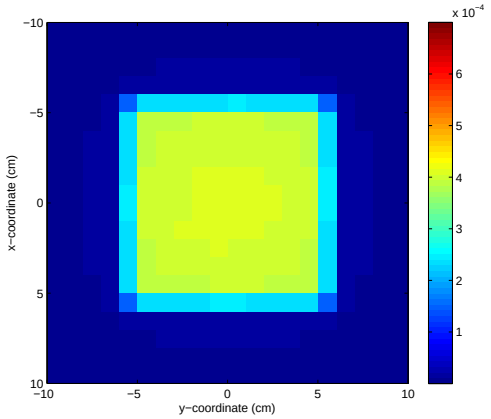

(b) depth=9.5cm

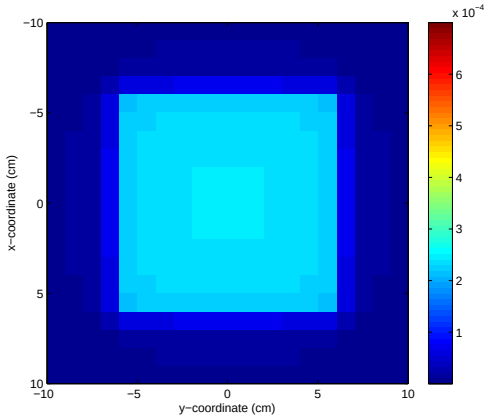

(c) depth=19.5cm

Figure 4: Axial kerma distributions at various depths from the reference solution

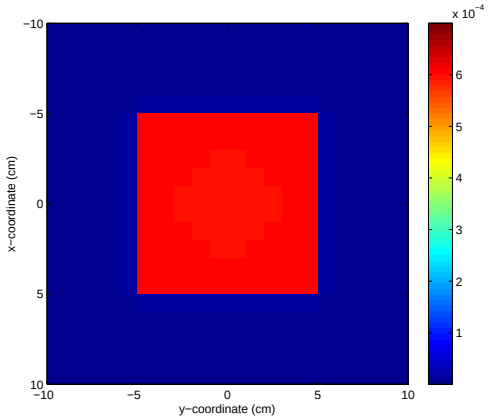

(a) depth=0.5cm

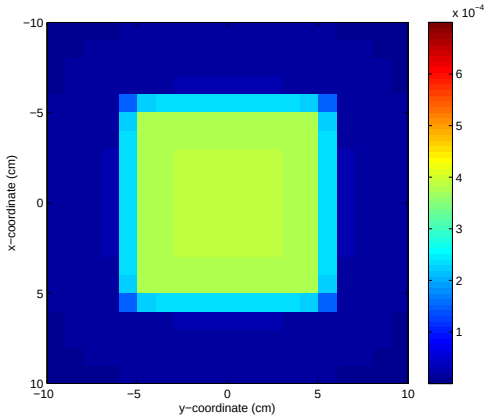

(b) depth=9.5cm

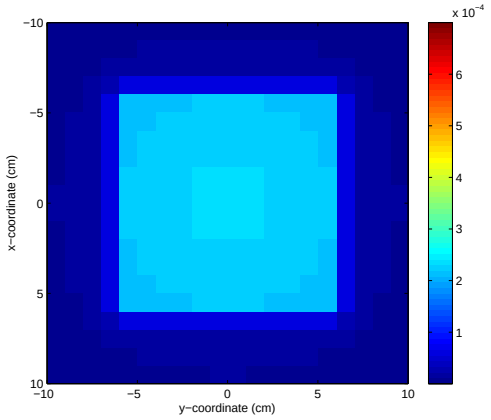

(c) depth=19.5cm

Figure 5: Axial kerma distributions at various depths from the COMET solution

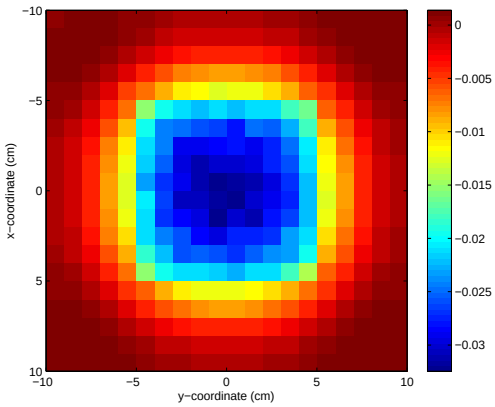

(a) depth=0.5cm

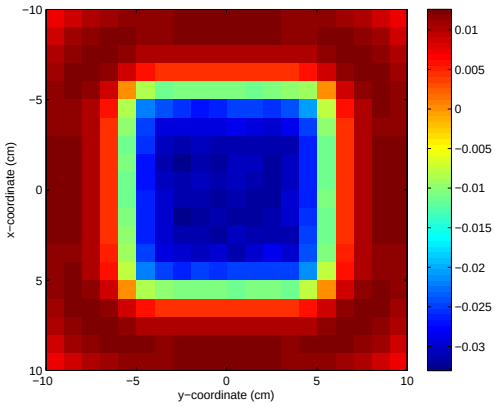

(b) depth=9.5cm

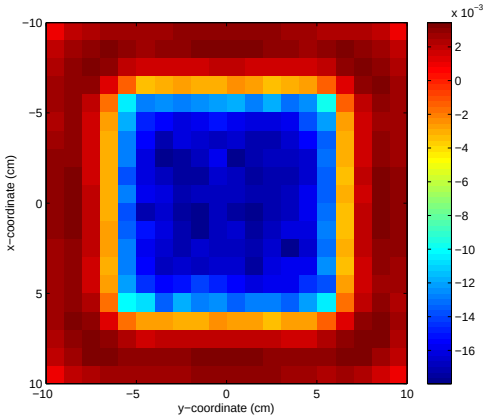

(c) depth=19.5cm

Figure 6: Error [units of K_{max}] for the axial kerma distributions at various depths

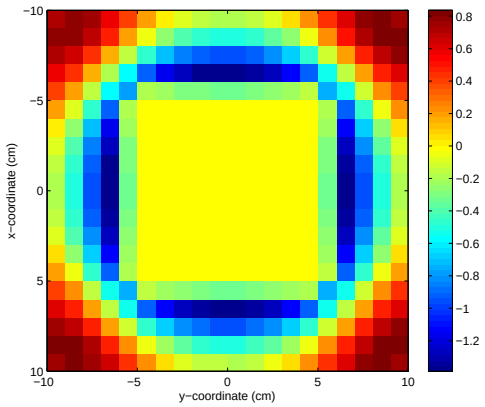

(a) depth=0.5cm

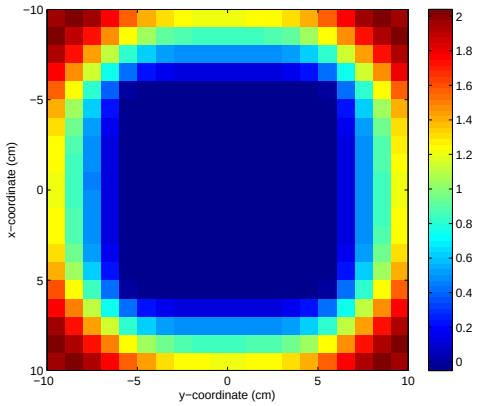

(b) depth=9.5cm

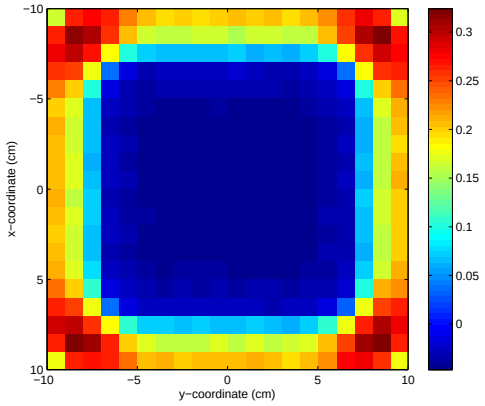

(c) depth=19.5cm

Figure 7: Relative error for the axial kerma distributions at various depths

Table 3: Running time comparison. The unit of time measure is defined as core-hours ≡ (# of cpu cores)*(# of hours on each). All calculations were performed on nodes with dual quad-core AMD Opterons clocked at 2 GHz.

task	**runtime**	**number of histories**
reference solution	84 core-hours	$8x10^9$
COMET solution	0.27 core-hours	-
source response calculation	5.4 core-hours	$6.4x10^9$
surface response calculation	128 core-hours	$1x10^8$

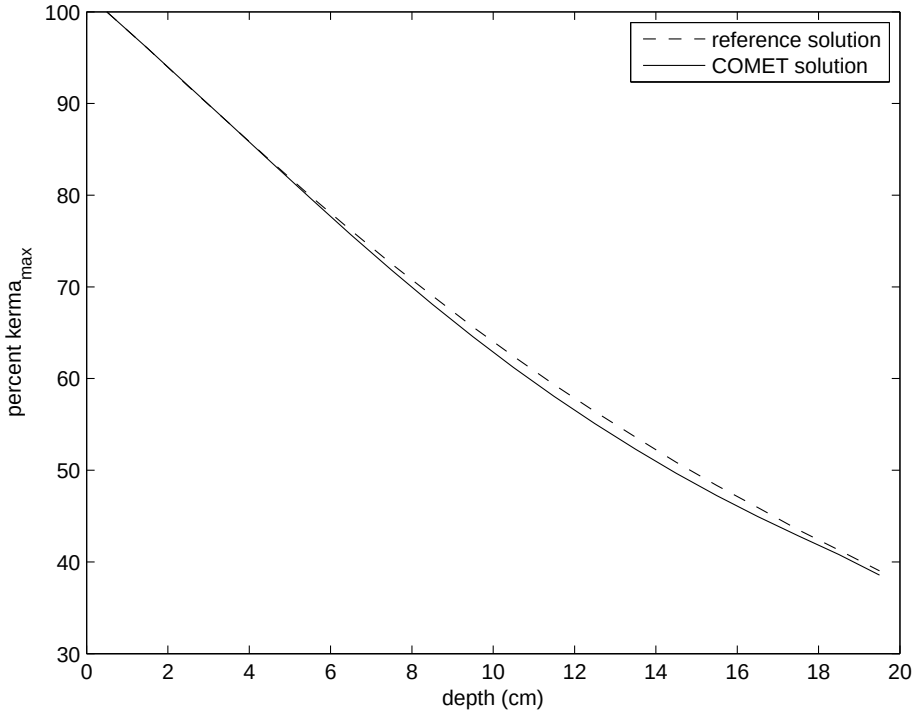

Figure 8: Percent Depth Kerma (PDK)

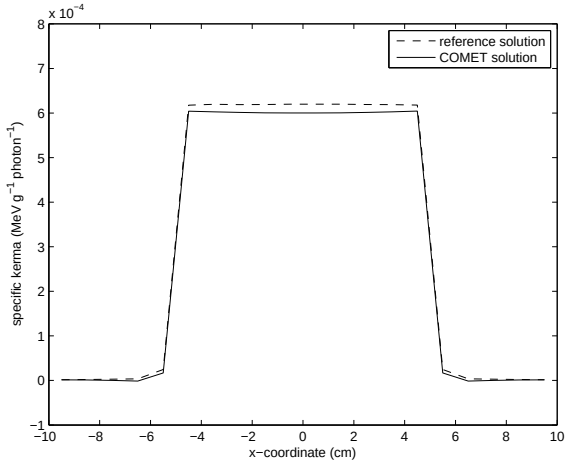

(a) depth=0.5cm

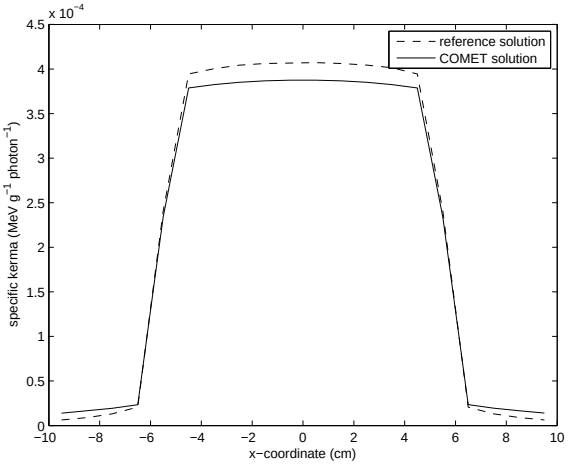

(b) depth=9.5cm

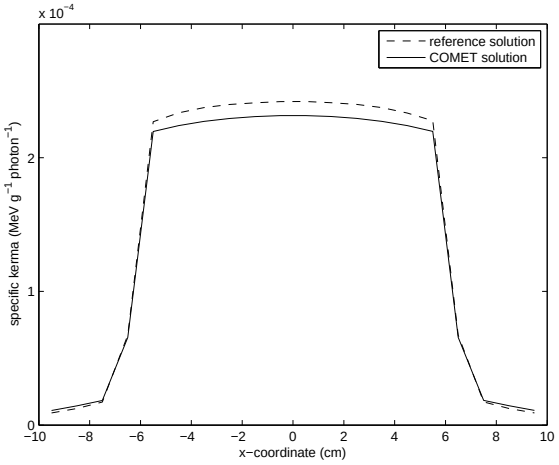

(c) depth=19.5cm

Figure 9: Beam profiles at various depths

CHAPTER VI

DISCUSSION

The COMET method clearly needs some work before it is ready to compete with Monte Carlo in accuracy. In this chapter, sources of error in the COMET calculation are identified, suggestions are made for future work, and concluding remarks are made.

6.1 Sources of Error

Three main sources of error exist in the COMET calculation. These are:

- source-response approximation error
- truncation error
- statistical uncertainty

The choice of a delta function as a basis for the source-response expansion is probably too weak for a couple of reasons. The first of these is that it does not capture any variation over space or angle of the source. That is, it ignores 5 out of 6 dimensions of the numerical phase space within each voxel. Since all of the photons are treated as if they are traveling parallel to the beams axis, there is an approximation error of 5.1°at the corner of the beam.

Both the source-response functions and the surface-response functions contain truncated expansions, and thus both are subject to truncation error. Previous work has suggested that an expansion to 3rd order in energy and azimuthal angle and to 2nd order space and polar angle is sufficient for near 1% error for a 2D photon-only geometry. This corresponds to $(4*4*3*3)^2*4 = 82,944$ coefficients per coarse mesh surface response function [15]. In the current work, with all second order expansions, $(3*3*3*3*3)^2*6 = 354,294$ coefficients per coarse mesh surface response function were calculated. Another difference

between this work and the above-mentioned benchmarking is the source term used. In previous work, there was no part of the phantom that was outside of the beam. The current work demonstrates that this is the most numerically difficult region for kerma calculation.

Since the response functions are calculated using Monte Carlo, statistical uncertainty inherently contributes to the error in a COMET calculation. However, based on past experience with 2D calculations, statistical error is not an important factor in the current work.

6.2 Suggestions for Future Work

The most important improvement to make for future work is to increase the expansion order of the both the volume-source response functions and the boundary response functions. This will result in a better transport approximation and will almost certainly improve the results. Closely related with this is the search for an optimal basis set. Since the response functions must be truncated at finite order, it is important to find efficient basis sets; that is basis sets that capture the important characteristics of the underlying distributions while using only a few terms.

The optimal selection of basis sets should be further investigated. Specifically, the balance of continuous and discrete approximations should be studied. For each dimension of the phase space, one must choose a continuous basis, a discrete basis, or a hybrid basis. Tools that automatically search the space of basis sets would be useful and instructive.

The effects of high-order statistical noise in response functions are not well understood at this point. Statistical theory should be developed along the lines of [8] to deal with the overall balance of statistical/truncation error in the COMET method.

Once the implementation is improved, it should be benchmarked with heterogeneous phantoms to simulate real-world treatment planning. Beyond this, addition of electron transport to the new method is the next logical step in development of COMET for medical physics applications. Aside from the uncollided flux calculation, all of the methods in this work have direct application to electron transport.

6.3 Conclusion

The COMET method for photon transport was theoretically extended to handle more general source terms, and a specific implementation of the new method was tested. The new test scenario is unprecedented in two ways:

- It is the first implementation of a 3D COMET method for photon transport.
- It is the first implementation of a photon COMET without the constraint of a flat source approximation.

The test implementation presented here is instructive in many ways, but more development is required. The theoretical foundation is laid, but this theory leaves many choices for its application. The key for future development lies in sorting through these choices to develop an efficient, accurate implementation.

REFERENCES

[1] Ahnesjö, A., "Collapsed cone convolution of radiant energy for photon dose calculation in heterogeneous media," *Medical Physics*, vol. 16, p. 577, 1989.

[2] Ahnesjö, A. and Aspradakis, M., "Dose calculations for external photon beams in radiotherapy," *Physics in Medicine and Biology*, vol. 44, pp. 99–155, 1999.

[3] Andreo, P., "Monte Carlo techniques in medical radiation physics," *Phys. Med*, vol. 36, no. 7, pp. 861–920, 1991.

[4] Attix, F., *Introduction to Radiological Physics and Radiation Dosimetry*. Wiley-Interscience, 1986.

[5] Blackburn, M. S., *Numerical Benchmarking of a Coarse-Mesh Transport (COMET) Method for Medical Physics Applications*. PhD thesis, Georgia Institute of Technology, August 2009.

[6] Boyer, A. and Schultheiss, T., "Effects of dosimetric and clinical uncertainty on complication-free local tumor control.," *Radiotherapy and oncology: journal of the European Society for Therapeutic Radiology and Oncology*, vol. 11, no. 1, p. 65, 1988.

[7] Gifford, K., Horton, J., Wareing, T., Failla, G., and Mourtada, F., "Comparison of a finite-element multigroup discrete-ordinates code with Monte Carlo for radiotherapy calculations," *Physics in Medicine and Biology*, vol. 51, no. 9, pp. 2253–2266, 2006.

[8] Griesheimer, D., Martin, W., and Holloway, J., "Convergence properties of Monte Carlo functional expansion tallies," *Journal of Computational Physics*, vol. 211, no. 1, pp. 129–153, 2006.

[9] Ilas, D. and Rahnema, F., "A Heterogeneous Coarse Mesh Transport Method," *Transport Theory and Statistical Physics*, vol. 32, pp. 445–471, 2003.

[10] Jacobs, F., Sundermann, E., De Sutter, B., Christiaens, M., and Lemahieu, I., "A fast algorithm to calculate the exact radiological path through a pixel or voxel space," *Journal of computing and information technology*, vol. 6, no. 1, pp. 89–94, 1998.

[11] Kawrakow, I., Rogers, D., Tessier, F., and Walters, B., "The EGSnrc code system: Monte Carlo simulation of electron and photon transport," *NRCC Report*, 2009.

[12] Lewis, E. E. and Miller, Jr., W. F., *Computational Methods of Neutron Transport*. John Wiley & Sons New York, 1984.

[13] Mackie, T. R., Scrimger, J. W., and Battista, J. J., "A convolution method of calculating dose for 15-mv x rays," *Medical Physics*, vol. 12, no. 2, pp. 188–196, 1985.

[14] Mosher, S. and Rahnema, F., "The Incident Flux Response Expansion Method for Heterogeneous Coarse Mesh Transport Problems," *Transport Theory and Statistical Physics*, vol. 35, no. 1, pp. 55–86, 2006.

[15] Satterfield, M. E., "Application of a heterogeneous coarse-mesh transport method (COMET) to radiation therapy problems," Master's thesis, Georgia Institute of Technology, December 2006.

[16] Sheikh-Bagheri, D. and Rogers, D., "Monte Carlo calculation of nine megavoltage photon beam spectra using the BEAM code," *Medical physics*, vol. 29, p. 391, 2002.

[17] Siddon, R., "Fast calculation of the exact radiological path for a three-dimensional CT array," *Medical Physics*, vol. 12, p. 252, 1985.

[18] Williams, M., Ilas, D., Sajo, E., Jones, D., and Watkins, K., "Deterministic photon transport calculations in general geometry for external beam radiation therapy," *Medical Physics*, vol. 30, p. 3183, 2003.

[19] Yuan, J., Jette, D., and Chen, W., "Deterministic photon kerma distribution based on the Boltzmann equation for external beam radiation therapy," *Medical Physics*, vol. 35, p. 4079, 2008.

[20] Zhang, D. and Rahnema, F., "Coupled Photon/Electron Coarse Mesh Transport Method for Dose Analysis in Tissues," in *Computational Medical Physics Working Group Workshop II*, (Gainesville, Florida USA), Sep 30–Oct 3, 2007.

[21] Zhao, H. and Reader, A., "Fast ray-tracing technique to calculate line integral paths in voxel arrays," in *2003 IEEE Nuclear Science Symposium Conference Record*, vol. 4, 2003.